Characterization of Chloride Ion Binding to Human Serum Albumin Using Cl NMR Null Point Spectral Analysis

William S. Price, Nien-Hui Ge, Luan-Ze Hong, and Lian-Pin Hwang*

Contribution from the Department of Chemistry, National Taiwan University, Taipei, Taiwan, Republic of China, and Institute of Atomic and Molecular Sciences, Academia Sinica, Taipei, Taiwan, Republic of China. *Received June 4, 1992*

Abstract: Cl NMR null point spectra have been applied to study the binding of chloride ions to human serum albumin. The density matrix formalism was used to simulate the null point spectra. We found that (1) the results were consistent with a weak and a strong class of binding sites; (2) relaxation at the weak sites could be modeled using a single correlation time for the fluctuation of the electric field gradient at the bound site, whereas binding at the strong site was modeled using a two-step model; (3) for the weak sites the enthalpy of dissociation was 20.2 kJ mol^{-1}, and at 310 K the correlation time was 3.4 ns; and (4) for the strong site at 310 K the slow correlation time was 35 ns and the upper limit for the fast correlation time was 0.5 ns, and the dissociation constant for the strong site was determined to be 0.1 M. This study shows that analysis of the fine spectral structure at the null point provides a more detailed source of motional information than the normally used measurements of longitudinal and transverse relaxation. This method also allows more accurate determination of correlation times and enables the interpretation of quadrupolar ion binding data when the relaxation is too nonexponential to allow the use of usual methods.

1. Introduction

Human serum albumin (HSA) has a molecular weight M_P of 66 439 and is the most abundant protein in blood plasma, with a concentration of about 42 g L^{-1}.[1] HSA is a single polypeptide chain consisting of 585 amino acids.[2,3] HSA provides about 80% of the colloid osmotic pressure of the blood and plays an important role in the binding and transport of endogenous and exogenous compounds.[4] In solution, HSA has the shape of a prolate ellipsoid with dimensions 144- × 45- × 22-Å.[5] Serum albumin exhibits a great deal of homology between different animal species. Extensive reviews of HSA and its properties may be found elsewhere.[1,6,7] HSA is known to bind a number of quadrupolar ions including Cl^-, Br^-, I^-, and Al^{3+}.[8,9]

Chloride ion binding to HSA and bovine serum albumin (BSA) has been studied by a variety of methods[10-15] including electrophoresis, equilibrium dialysis, ion-selective electrodes, and NMR.[8,16-19] It has been shown that there is little or no difference between the chloride ion binding properties of HSA and BSA.[12,15] The results of previous NMR studies suggest that there are two classes of chloride binding sites on HSA: a small number of strong binding sites, to which chloride binding can be inhibited by stoichiometric amounts of sodium dodecyl sulfate (SDS),[8,19] and weak (SDS-insensitive) binding sites. The Cl^- exchange between protein binding sites and the bulk solution state is believed to be in the fast exchange limit,[16,19] with the free population p_f greatly exceeding the bound population p_b (at least for the chloride concentrations used to date in NMR experiments).

^{35}Cl and ^{37}Cl NMR provide a convenient means for studying the exchange and binding of chloride ions between free solution and protein binding sites.[20,21] Previous NMR studies of chloride binding to albumin have been performed at low magnetic field strengths (≤2.5 T) and have relied upon measuring the excess longitudinal or transverse relaxation rates (i.e., the difference between the measured relaxation rate and that measured in the absence of protein) resulting from the chloride ions binding to HSA.[8,16-19,22] The excess relaxation data were then analyzed to extract the fluctuation correlation time of electronic field gradient at the bound sites τ_b. The bound population occurs in the relaxation equations as a product of the square of the quadrupolar coupling constant of the bound sites χ_b (i.e., $\chi_b = e^2Qq/h$, where eq is the electric field gradient at the nucleus at the bound site, eQ is the electric quadrupole moment of the nucleus, and h is the Planck constant). This product forms a constant, and the product can only be separated if one of the two terms can be independently determined. However, generally the flucutation correlation time of the electric field gradient and the quadrupole coupling constant at the free site can be independently determined. Chloride ions bound to HSA are outside the extreme narrowing condition (i.e., $\omega_0\tau_b \ll 1$, where ω_0 is the Larmor frequency of the chloride ions), and thus the relaxation at the bound site is nonexponential.[23] However, the observed relaxation is a function of the chloride ions in both free and bound states and the exchange rate. Generally the longitudinal relaxation appears to be exponential but the transverse relaxation does not (see below). A useful single exponential approximation has been devised for the case $\omega_0\tau_b \leq 1.5$.[24] However, with NMR spectrometers having increasingly larger static magnetic fields, the assumption of the relaxation approximating a single exponential process becomes less realistic.

* Author to whom correspondence should be addressed.

(1) Peters, T., Jr. *Adv. Protein Chem.* **1985**, *37*, 161-245.
(2) Behrens, P. Q.; Spiekerman, A. M.; Brown, J. R. *Fed. Proc.* **1975**, *34*, 591.
(3) Meloun, B.; Moravek, L.; Kostka, V. *FEBS Lett.* **1975**, *58*, 134-137.
(4) Russell, N. J.; Powell, G. M.; Jones, J. G.; Winterburn, P. J.; Basford, J. M. *Blood Biochemistry*; Croom Helm: London, 1982.
(5) Yang, J. T. *Adv. Protein Chem.* **1961**, *16*, 323-400.
(6) Kragh-Hansen, U. *Pharmacol. Rev.* **1981**, *33*, 17-53.
(7) Kragh-Hansen, U. *Dan. Med. Bull.* **1990**, *37*, 57-84.
(8) Norne, J.-E.; Hjalmarsson, S. G.; Lindman, B.; Zeppezauer, M. *Biochemistry* **1975**, *14*, 3401-3408.
(9) Fatemi, S. J. A.; Kadir, F. H. A.; Moore, G. R. *Biochem. J.* **1991**, *280*, 527-532.
(10) Scatchard, G.; Scheinberg, I. H.; Armstrong, S. H., Jr. *J. Am. Chem. Soc.* **1950**, *72*, 535-540.
(11) Alberty, R. A.; Marvin, H. H., Jr. *J. Am. Chem. Soc.* **1951**, *73*, 3220-3223.
(12) Carr, C. W. *Arch. Biochem. Biophys.* **1952**, *40*, 286-294.
(13) Carr, C. W. *Arch. Biochem. Biophys.* **1953**, *46*, 417-423.
(14) Scatchard, G.; Coleman, J. S.; Shen, A. L. *J. Am. Chem. Soc.* **1957**, *79*, 12-20.
(15) Scatchard, G.; Yap, W. T. *J. Am. Chem. Soc.* **1964**, *86*, 3434-3438.
(16) Norne, J. E.; Bull, T. E.; Einarsson, R.; Lindman, B.; Zeppezauer, M. *Chem. Scr.* **1973**, *3*, 142-144.
(17) Bull, T. E.; Halle, B.; Lindman, B. *FEBS Lett.* **1978**, *86*, 25-28.
(18) Rose, K.; Bryant, R. G. *J. Magn. Reson.* **1978**, *31*, 41-47.
(19) Halle, B.; Lindman, B. *Biochemistry* **1978**, *17*, 3774-3781.
(20) Forsén, S.; Lindman, B. *Methods Biochem. Anal.* **1981**, *27*, 289-486.
(21) Price, W. S.; Kuchel, P. W.; Cornell, B. A. *Biophys. Chem.* **1991**, *40*, 329-337.
(22) Bull, T. E.; Norne, J.-E.; Reimarsson, P.; Lindman, B. *J. Am. Chem. Soc.* **1978**, *100*, 4643-4647.
(23) Hubbard, P. S. *J. Chem. Phys.* **1970**, *53*, 985-987.
(24) Bull, T. E. *J. Magn. Reson.* **1972**, *8*, 344-353.

0002-7863/93/1515-1095$04.00/0

From an SDS titration at pH 7.4, Norne and co-workers[8] found that there were 9 ± 1 binding sites on each albumin molecule in the strong binding limit. With this value and the assumption that a single effective correlation time was sufficient to define the fluctuation of the electric field gradient at the strong site, they determined the correlation time to be 11.4 ns and the quadrupole coupling constant of the strong site χ_s to be 1.2 MHz using Bull's single exponential approximation.[24] Rose and Bryant determined the correlation time of the strong site to be 16 ns at 300.5 K and pH 7.1.[18] Halle and Lindman concentrated on the nature of the strong class of binding sites and considered the ellipsoidal shape of HSA in solution in analyzing their NMR relaxation data.[19] From an SDS titration at pH 7.2, they found that there were 7 ± 1 chloride binding sites per HSA in the strong binding limit. They associated these sites with lysine and arginine residues in the amino acid sequence of HSA. Bull and co-workers[17,22] suggested that internal motion at the strong site might explain why the apparent correlation times for the strong site determined from analysis of Cl^- NMR relaxation data were considerably smaller than those calculated or derived from dielectric relaxation measurements for the albumin molecule. They suggested that binding sites on the protein surface possess a considerable degree of internal flexibility and that this internal flexibility may affect the biological function.[17,22] Bull and co-workers[17,22] analyzed ^{35}Cl relaxation data, considering internal motion of the strong binding sites in terms of a simple model in which the chloride ion is attached to a rod which moves about in a conical hole embedded in the protein.[25] However, the theory gave a number of self-consistent sets of parameters, and in order to determine just one set of parameters an independent determination of χ_s for the bound site was necessary; the researchers had to use an overall reorientational correlation time derived from dielectric relaxation measurements.

Null point spectra were first observed for dipolar relaxation in methyl protons (in which the quartet of spin levels are formally equivalent to an isolated spin-$^3/_2$ nucleus such as chlorine) by Haslinger and co-workers.[26-29] Subsequently this effect was analyzed in terms of cross-dipolar interactions by Lee and Hwang.[30] Null point spectra for quadrupolar nuclei undergoing chemical exchange were first found experimentally by Urry and co-workers.[31,32] Recently we have observed and successfully analyzed the relaxation for spin-$^3/_2$ nuclei in homogeneous systems[33] and involved in chemical exchange processes.[34] The fine structure in the null point is a consequence of the evolution of the rank 3 multipole (see below). The maximum value for the rank 3 multipole and the minimum absolute amplitude of the rank 1 multipole occur at approximately the same time as the null point in the inversion–recovery experiment (for example, see Figure 2 in Price et al.[33]). The asymmetry in the null point results from the dynamic frequency shift.[33,34] Thevand and Werbelow[35] have recently discussed the effects of the dynamic frequency shift in null point spectra of methyl groups.

In the present work the fine spectral structure observed near the null point in inversion–recovery experiments was used in combination with longitudinal and transverse relaxation measurements to determine the relevant NMR parameters of the two classes of chloride binding sites and the enthalpy of dissociation of the weak binding site. The fine spectral structure at the null point also provides a convenient means to observe the dynamic frequency shift. The shape of the null point spectra contains information complementary to normal longitudinal and transverse relaxation measurements. In the analysis of the null point spectra the shape and the intensity relative to that of the fully relaxed spectrum were considered. Specifically, the NMR relaxation data obtained in the presence of SDS were analyzed to give the fluctuation correlation time at the weak binding site τ_w, but since the chloride ion population at the weak sites p_w could not be determined, the quadrupole coupling constant at the weak site χ_w could only be given as $p_w\chi_w^2$. In analyzing the data from the SDS-sensitive sites a two-step model-free approach was applied to account for internal motion at the binding site. This model required a slow correlation time (τ_{ss}), a fast correlation time (τ_{sf}), and an order parameter (A). More than one set of parameters were found to be consistent with the observed relaxation rates. However, only a much smaller group of these parameters could fit the line shapes of the null point spectra. Compared to previous NMR studies of Cl^- binding, no assumptions about the degree of exponentiality of the relaxation processes were made since a full density matrix formulation has been used.

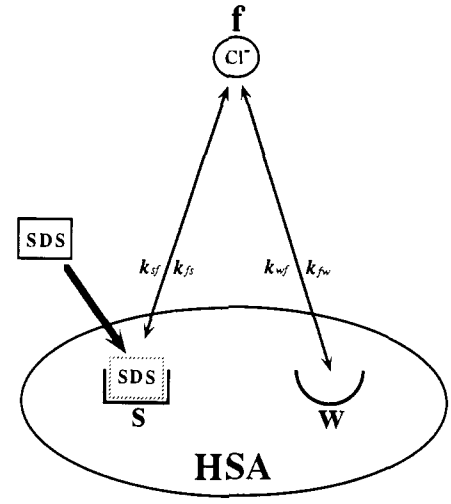

Figure 1. Schematic representation of chloride ion binding to HSA. The chloride ion exchange between the free (f) and weak (w) sites occurs independently of the exchange between the free and strong (s) sites. There are n_s and n_w strong and weak chloride binding sites per HSA molecule. The population of chloride ions at the free, strong, and weak sites is denoted by p_f, p_s, and p_w, respectively. The chloride ion binding to the strong site may be inhibited by stoichiometric amounts (with respect to the number of strong binding sites) of SDS. k_{xy} is the microscopic rate constant for transfer from site x to site y (where x, y = f, s, w). Direct exchange between sites s and w is neglected because it would be very slow, as it is limited by the Cl^- ion diffusion rate on the HSA surface.

2. Theory

2.1. Kinetics of Ion Binding. A brief coverage of the relevant kinetics of ion binding is given in Appendix 1. More complete accounts may be found elsewhere (e.g., refs 36 and 37). As the present work involves concentrated solutions of varying ionic strength, the activities instead of the concentrations of the species were used in the calculations (see Appendix 1). In the activity calculations, we have taken the net charge, Z_P on HSA to be −23, the effective radius of HSA r_P as 3.53 nm, the partial specific volume of HSA ν_P as 1.67 mL g^{-1},[38] the net charge of the chloride ion Z_{Cl} to be −1, and the radius of the chloride ion r_{Cl} as 0.18 nm.

The model for chloride ion binding used in the present work is given schematically in Figure 1. In our model of chloride ion binding to HSA the following assumptions were made: (1) There

(25) Bull, T. E. *J. Magn. Reson.* **1978**, *31*, 453–458.
(26) Haslinger, E.; Lynden-Bell, R. M. *J. Magn. Reson.* **1978**, *31*, 33–40.
(27) Haslinger, E.; Robien, W. *J. Am. Chem. Soc.* **1980**, *102*, 1237–1241.
(28) Haslinger, E.; Robien, W.; Schölm, R. *J. Organomet. Chem.* **1980**, *194*, 331–335.
(29) Haslinger, E.; Kalchhauser, H.; Robien, W. *J. Mol. Liq.* **1984**, *28*, 223–228.
(30) Lee, T. S.; Hwang, L. P. *J. Magn. Reson.* **1990**, *89*, 51–59.
(31) Urry, D. W.; Trapane, T. L.; Brown, R. A.; Venkatachalam, C. M.; Prasad, K. U. *J. Magn. Reson.* **1985**, *65*, 43–61.
(32) Urry, D. W.; Trapane, T. L.; Venkatachalam, C. M.; Prasad, K. U. *J. Am. Chem. Soc.* **1986**, *108*, 1448–1454.
(33) Price, W. S.; Ge, N. H.; Hwang, L. P. *J. Magn. Reson.* **1992**, *98*, 134–141.
(34) Ge, N. H.; Price, W. S.; Hong, L. Z.; Hwang, L. P. *J. Magn. Reson.* **1992**, *97*, 656–660.
(35) Thevand, A.; Werbelow, L. *J. Magn. Reson.* **1992**, *97*, 192–193.
(36) Marshall, A. G. *Biophysical Chemistry*; Wiley: New York, 1978; pp 70–84.
(37) Chang, R. *Physical Chemistry with Applications to Biological Systems*, 2nd ed.; MacMillan Publishing Co., Inc.: New York, 1981; pp 249–250.
(38) Minton, A. P.; Edelhoch, H. *Biopolymers* **1982**, *21*, 451–458.

are n_w equivalent weak binding sites, and the SDS titration curves (see below) suggest that there are n_s equivalent strong binding sites. (2) The Cl^- exchange between sites s and f occurs independently of the Cl^- exchange between sites w and f since the free population is much larger than the bound populations (i.e., $p_f \approx 1$) and the exchange between sites s and w would be very slow as it is limited by the Cl^- ion diffusion rate on the protein surface. The principle of detailed balancing of the exchange process demands that[39]

$$p_f k_{fw} = p_w k_{wf} \tag{1a}$$

and

$$p_f k_{fs} = p_s k_{sf} \tag{1b}$$

where k_{fw} is the microscopic rate constant for transfer from site f to site w, k_{wf} is the microscopic rate constant from site w to f, k_{fs} is the microscopic rate constant for transfer from site f to site s, k_{sf} is the microscopic rate constant from site s to f, and p_s is the chloride ion population at the strong sites. We then define the exchange times for the weak sites τ_{exw} and the strong sites τ_{exs} as

$$\tau_{exw} = \frac{p_w}{k_{fw}} = \frac{p_f}{k_{wf}} \tag{2a}$$

$$\tau_{exs} = \frac{p_s}{k_{fs}} = \frac{p_f}{k_{sf}} \tag{2b}$$

In the fast exchange limit the conditions $|\delta_f - \delta_w|\tau_{exw} \ll 1$ and $|\delta_f - \delta_s|\tau_{exs} \ll 1$ hold, where δ_f, δ_w, and δ_s are the chemical shifts in angular frequency units of free, weak, and strong sites, respectively.

Using the above assumptions the probability distributions for sites w and s may be expressed by (see Appendix 1)

$$p_w = \frac{n_w C_P a_{Cl}}{C_{Cl}(K_w \Phi + a_{Cl})} \tag{3a}$$

$$p_s = \frac{n_s C_P a_{Cl}}{C_{Cl}(K_s \Phi + a_{Cl})} \tag{3b}$$

where a_{Cl} is the activity of the free chloride ions, $K_w(K_s)$ is the dissociation constants of Cl^- for the weak (strong) binding sites, Φ (see Appendix 1) corrects for the effects of protein activity, and $C_{Cl}(C_P)$ is the total chloride (protein) concentration, respectively. For the case of two-site exchange (i.e., chloride ions binding to HSA in the presence of SDS), K_w can be related to k_{fw} and k_{wf} using eqs 1 and 3 by

$$\frac{k_{fw}}{k_{wf}} = \frac{n_w C_P a_{Cl}}{C_{Cl}(K_w \Phi + a_{Cl}) - n_w C_P a_{Cl}} \tag{4}$$

By analogy, similar equations can be derived for a three-site exchange (i.e., chloride ions binding to HSA in the absence of SDS).

2.2. Relaxation Theory. The basic relaxation theory is the same as that used in our previous work.[33,34] The relaxation data from the inversion–recovery experiments (i.e., null point spectra and longitudinal relaxation measurements) were simulated using a complete formulation of the relaxation processes (i.e., both longitudinal and transverse) occurring throughout the inversion–recovery pulse sequence and the subsequent acquisition period. As before,[30,33,34] the relaxation equations used were simplified by expressing the density matrix of the spin system in terms of state multipoles.[40,41] A rank k multipole with tensorial component m is denoted by σ_m^k. State multipoles are nothing more than specific linear combinations of the normal density matrix elements such that the combinations take advantage of rotational symmetries. The relevant properties of state multipoles are summarized in Appendix 2. Although the following exchange equations are written in terms of state multipoles, the same equations hold for traditional density matrix calculations. The exchange equations presented here are general; however, for convenience the components of the equations are labeled with respect to their use in the current work. As in our previous study of chloride binding to HSA in the presence of SDS,[34] a single correlation time was used to represent relaxation at the weak sites. However, a single correlation time was found to be insufficient to model the chloride relaxation at the strong site. To account for internal motion at the strong site and yet to avoid over-interpretation of the relaxation data, a two-step model-free approach was used (see below).

2.2.1. Density Matrix Equation of Motion for Two-Site Exchange. The density matrix equation for longitudinal relaxation including exchange between a free site (f) and a weak binding site (w) is described by the following rate equation[39]

$$\frac{d}{dt}\begin{bmatrix}\rho_f\\ \rho_w\end{bmatrix} = \begin{bmatrix}-R_f - k_{fw}I & k_{wf}I\\ k_{fw}I & -R_w - k_{wf}I\end{bmatrix}\begin{bmatrix}\rho_f\\ \rho_w\end{bmatrix} \tag{5}$$

where I is a unit matrix and R_f (or R_w) is the Redfield relaxation matrix for the longitudinal components of the state multipoles in site f (or w).[33,42] The column density matrices ρ_f and ρ_w are defined as column density matrices of state multipoles in sites f and w, respectively, by

$$\tilde{\rho}_f \equiv [(\sigma_0^1)_f, (\sigma_0^3)_f] \text{ and } \tilde{\rho}_w \equiv [(\sigma_0^1)_w, (\sigma_0^3)_w]$$

In order that the longitudinal components of the state multipoles have achieved thermal equilibrium values at infinite time, the difference between σ_0^k and its equilibrium value (see below) is substituted for σ_0^k in solving eq 5. Similarly, the transverse relaxation equation is defined by

$$\frac{d}{dt}\begin{bmatrix}\rho'_f\\ \rho'_w\end{bmatrix} = \begin{bmatrix}-R'_f - k_{fw}I - i(\omega_0 - \delta_f)I & k_{wf}I\\ k_{fw}I & -R'_w - k_{wf}I - i(\omega_0 - \delta_w)I\end{bmatrix}\begin{bmatrix}\rho'_f\\ \rho'_w\end{bmatrix} \tag{6}$$

where R'_f (or R'_w) is the Redfield relaxation matrix for the transverse components of the state multipoles in site f (or w).[33,42] Unlike the longitudinal relaxation matrices, which are real, the transverse relaxation matrices are complex. The real parts give rise to the relaxation rate, and the imaginary parts give rise to the dynamic frequency shift. The column density matrices are defined by

$$\tilde{\rho}'_f \equiv [(\sigma_1^1)_f, (\sigma_1^3)_f] \text{ and } \tilde{\rho}'_w \equiv [(\sigma_1^1)_w, (\sigma_1^3)_w]$$

To guarantee the validity of eqs 5 and 6, the condition $\tau_{exw} \gg \tau_w$ must hold.

2.2.2. Density Matrix Equation of Motion for Three-Site Exchange. The density matrix equation for longitudinal relaxation including exchange between the free, strong, and weak sites is described by the rate equation

$$\frac{d}{dt}\begin{bmatrix}\rho_f\\ \rho_s\\ \rho_w\end{bmatrix} = \begin{bmatrix}-R_f - (k_{fs} + k_{fw})I & k_{sf}I & k_{wf}I\\ k_{fs}I & -R_s - k_{sf}I & 0\\ k_{fw}I & 0 & -R_w - k_{wf}I\end{bmatrix}\begin{bmatrix}\rho_f\\ \rho_s\\ \rho_w\end{bmatrix} \tag{7}$$

where

(39) Binsch, G. In *Dynamic Nuclear Magnetic Resonance Spectroscopy*; Jackman, L. M., Cotton, F. A., Eds.; Academic Press: New York, 1975; pp 45–81.

(40) Blum, K. *Density Matrix Theory and Applications*; Plenum: New York, 1981.

(41) Sanctuary, B. C. *J. Magn. Reson.* **1985**, *61*, 116–129, and references therein.

(42) Einarsson, L.; Westlund, P. O. *J. Magn. Reson.* **1988**, *79*, 54–65. The longitudinal relaxation matrix given in this reference has a typographical error which has been corrected in 33.

$\tilde{p}_f \equiv [(\sigma_0^1)_f, (\sigma_0^3)_f]$, $\tilde{p}_s \equiv [(\sigma_0^1)_s, (\sigma_0^3)_s]$, and $\tilde{p}_w \equiv [(\sigma_0^1)_w, (\sigma_0^3)_w]$

The density matrix equation for transverse relaxation including exchange between the free, strong, and weak sites is described by the rate equation

$$\frac{d}{dt}\begin{bmatrix} \rho'_f \\ \rho'_s \\ \rho'_w \end{bmatrix} = \begin{bmatrix} -R'_f-(k_{fs}+k_{fw})I-i(\omega_0-\delta_f)I & k_{sf}I & k_{wf}I \\ k_{fs}I & -R'_s-k_{sf}I-i(\omega_0-\delta_s)I & 0 \\ k_{fw}I & 0 & -R'_w-k_{wf}I-i(\omega_0-\delta_w)I \end{bmatrix} \times \begin{bmatrix} \rho'_f \\ \rho'_s \\ \rho'_w \end{bmatrix} \quad (8)$$

where

$\tilde{p}'_f \equiv [(\sigma_1^1)_f, (\sigma_1^3)_f]$, $\tilde{p}'_s \equiv [(\sigma_1^1)_s, (\sigma_1^3)_s]$, and $\tilde{p}'_w \equiv [(\sigma_1^1)_w, (\sigma_1^3)_w]$

To guarantee the validity of eqs 7 and 8, the conditions $\tau_{exs} \gg \tau_{ss}$ and $\tau_{exw} \gg \tau_w$ must hold. In our particular case the spectral density functions used in R_s and R'_s defined in Price et al.[33] are replaced by those derived in the two-step model (see Section 2.2.3 and Appendix 3).

2.2.3. Two-Step Model-Free Approach. The internal motion at the strong binding site is accounted for by a modification of the approach of Halle and Wennerström.[43] The spectral density functions relevant to this model are given in Appendix 3. Experimentally, it was observed from the fitting of null point spectra that the parameter sets used satisfied the following two relations

$$p_s\chi_s^2(1 + \eta^2/3 - A^2)\tau_{sf} \equiv C_1 \quad (9a)$$

$$p_s\chi_s^2A^2\tau_{ss} \equiv C_2 \quad (9b)$$

where C_1 and C_2 are constants to be determined and η is the asymmetry parameter. Later it was noted that in the system studied the conditions $\omega_0\tau_{sf} \ll 1$ and $\omega_0\tau_{ss} \gg 1$ held (see below) and that in this limit J_{1f} and J_{2f} can both be replaced by J_{0f} and then J_{0f} and J_{0s} will dominate the relaxation process (see Appendix 3). This then causes the relationships expressed in eq 9.

2.3. Simulation of Null Point Spectra. Here we describe the use of the above theory in simulating the free induction decay obtained from the inversion–recovery rf pulse sequence (i.e., π-τ-$\pi/2$-Acq) in the case of two-site exchange. Null point spectra are merely those spectra acquired at τ values such that the net magnetization is near 0. The equilibrium state multipoles can be calculated from the corresponding density matrix elements (see Appendix 2, eq A.2.1) to be

$$(\sigma_0^1)_{eq} = \frac{(5)^{1/2}\gamma\hbar B_0}{(2I+1)kT}$$

and

$$(\sigma_0^3)_{eq} = 0$$

Since we have exchanging species, the individual multipoles must be appropriately population weighted. The effects of the π pulse were then calculated (See Appendix 2, eq A.2.2.), and thus immediately after the π pulse and including population weighting the state multipoles are

$$(\sigma_0^k)_{f(w)} = -p_{f(w)}(\sigma_0^k)_{eq}$$

where $(\sigma_0^k)_{eq}$ is the equilibrium state multipole. Equation 5 is then used to follow the evolution of the longitudinal magnetization and the "motional" behavior of the spins during the delay time τ. The $\pi/2$ pulse transforms the longitudinal state multipoles into transverse state multipoles. The rf pulses are considered to be δ functions and so do not cause mixing of the site w and f multipoles. The effects of the $\pi/2$ pulse were calculated (See Appendix 2, eq A.2.2.), and the result formed the initial condition for calculating the evolution of transverse magnetization and the motional behavior of spins during the acquisition period using eq 6. The time evolution of the following term corresponds to the free induction decay.

$$[(\sigma_1^1)_f + (\sigma_1^1)_w]$$

The spectral line shape is related to the real part of the Fourier–Laplace transform of this term, which evolves during the acquisition period. The procedure is similar for three-site exchange, except that the initial condition after the π pulse now involves population weighting of sites f, s, and w and the assumption that the rf pulses do not cause mixing between the multipoles of sites f, s, and w. Also, eq 7 is substituted for eq 5 and eq 8 is substituted for eq 6, and the spectral line shape is now related to the real part of the Fourier–Laplace transform of the following term which evolves during the acquisition period.

$$[(\sigma_1^1)_f + (\sigma_1^1)_s + (\sigma_1^1)_w]$$

In fitting null point spectra resulting from three-site exchange, an initial estimate for p_s of 0.003 15 was calculated from eq 3b, the concentrations of chloride ion and HSA used in the null point samples, and the assumption that all of the SDS-sensitive sites were occupied by chloride ions; clearly this value constitutes an upper bound for p_s. Initial estimates for χ_s, A, τ_{sf}, and τ_{ss} were then provided, and the constrained nonlinear optimization package of Matlab-386 (The Mathworks Inc., MA), which is based on the sequential quadratic programming algorithm, was used to find the set of parameters that fit the peak intensity versus τ delay in the inversion–recovery pulse sequence and the line widths at one-half and one-third height of the fully relaxed spectrum. These parameters were then used as a starting point for simulating the null point spectra. The value of χ_s was given a minor adjustment to make the τ values coincide with the null point spectra. The constraints used for assessing the goodness of fit of the null point simulations were the dynamic frequency shift, the time dependence of the fine structure of the null point spectra, and the relative intensities of the null point spectra to that of the fully relaxed spectrum. At the end of the fitting process the parameters obtained gave good fits to (1) the null point line shapes, (2) the longitudinal relaxation data, and (3) the line shape of the fully relaxed spectrum. The fitting procedure for the two-site model was similar.

2.4. Evaluation of Longitudinal Relaxation Measurements. Longitudinal relaxation was simulated using the full density matrix formalism (see above), and the net magnetization derived from this was well described by a single exponential. Simulation of longitudinal relaxation measurements derived from Cl^- ions involved in two-site exchange was in essence the same as that for evaluating the null point spectra except that the intensity of the spectral line obtained from the term

$$[(\sigma_1^1)_f + (\sigma_1^1)_w]$$

at respective τ delays in the inversion–recovery rf pulse sequence was used to represent the magnetization. The function $b_1 + b_2\exp(-\tau/T_1)$, where b_1 and b_2 are constants, was then regressed onto the magnetization versus τ data to obtain values for T_1. For simulating longitudinal relaxation measurements derived from Cl^- ions involved in three-site exchange, the same procedure was used except that the intensity was calculated from the following term

$$[(\sigma_1^1)_f + (\sigma_1^1)_s + (\sigma_1^1)_w]$$

3. Experimental Section

Human serum albumin (fraction V) and Tris-HCl (THAM hydrochloride, tris(hydroxymethyl)aminomethane hydrochloride) were obtained from Sigma, MO. NaCl and Tris were obtained from Fisher, NJ. D_2O was obtained from Isotec, OH, and Merck, Darmstadt, Germany. SDS was obtained from BDH, Poole, England. Sodium sulfate was obtained from Yakuri Pure Chemicals Co., Ltd., Osaka, Japan. Sodium thiocyanate was from Riedel-de Haën, Hannover, Germany.

(43) Halle, B.; Wennerström, H. *J. Chem. Phys.* **1981**, *75*, 1928–1943.

Table I. Longitudinal Relaxation Times (T_{1f}) and Corresponding Fluctuation Correlation Times for the Electric Field Gradient at the Nucleus (τ_f) for Free Chloride (1 M) and the Measured Longitudinal Relaxation Times (T_1) and Parameters Used To Fit the ^{35}Cl Null Point Spectra of the SDS-Containing Null Point Sample at Each Temperature

T (K)	T_{1f} (ms)	τ_f (ps)	T_1 (ms)	$p_w\chi_w^{2\,a}$ (kHz^2)	$p_w{}^b$	$\tau_w{}^c$ (ns)
316	40.6	2.1	18.0	5270	0.020	3.36
310	36.3	2.3	15.2	6260	0.024	3.40
298	27.3	3.1	12.0	7980	0.031	3.48
288	20.4	4.1	9.0	11200	0.043	3.55
283	18.1	4.6	7.7	13000	0.050	3.60
278	14.6	5.7	6.3	15900	0.061	3.65

[a] Values have a 3% error associated with them. [b] Upper bound value. [c] Values have a 10% error associated with them.

A null point sample without SDS was prepared by dissolving HSA, NaCl, Tris, and Tris-HCl in D_2O to give HSA 0.45 mM, Tris 8 mM, Tris-HCl 42 mM, and NaCl 1 M. The pH was 7.5 (uncorrected for isotope effect). A second null point sample was similarly prepared but with an SDS concentration of 7.2 mM, which was sufficient to block the SDS-sensitive chloride binding sites (see below). Samples containing HSA, with and without SDS, containing various chloride or HSA concentrations were similarly prepared. Protein concentrations were determined spectrometrically, using an extinction coefficient of 36 500 M^{-1} cm^{-1} at 279 nm.[44]

Protein-free samples were also prepared. The pH of the 1 M NaCl protein-free sample (uncorrected for isotope effect) was 7.7. The accessibility of the chloride ion content of the Tris buffer in a protein-free sample was determined to be 100% using a chloride electrode (Orion 9417BN, Orion Research Inc., MA).

The ^{35}Cl NMR measurements were performed on Bruker AM-400, MSL-300, and MSL-90 spectrometers operating at 39.21, 29.41, and 8.83 MHz, respectively. ^{37}Cl NMR measurements were performed at 24.48 MHz using a Bruker MSL-300 spectrometer. Transverse relaxation measurements were obtained from line width measurements or using the Hahn spin–echo pulse sequence. The null point spectra and longitudinal relaxation measurements were obtained using the inversion–recovery pulse sequence. ^{35}Cl and ^{37}Cl NMR null point spectra were acquired only at 29.41 and 24.48 MHz due to signal-to-noise limitations of the MSL-90 spectrometer and a lack of a 10-mm heteronuclear probe for the AM-400 spectrometer. Typical ^{35}Cl and ^{37}Cl acquisition parameters were a spectral width of 5000 Hz, digitized into 4K data points with a $\pi/2$ pulse length of about 30 μs. Each null point spectra is the average of at least 11 000 scans for ^{35}Cl and 45 000 scans for ^{37}Cl. A delay of at least $10T_1$ was used for all of the measurements. The meausred T_1 values have about 7% error associated with them. The NMR probe temperatures were checked using either ethylene glycol or methanol.[45,46]

4. Results

4.1. Estimation of χ_f and τ_f. As in our previous work,[34] a value for τ_f of 2.3 ps and a value for χ_f of 1.7 MHz were estimated from the ^{35}Cl T_1 value of 36.3 ms at 29.4 MHz for free chloride (1 M) at 310 K in conjunction with results obtained by Hertz[47,48] and the assumption that the fluctuation of the electric field gradient at the chloride nucleus is caused by the reorientational motion of the water molecules in the first hydration layer.[48,49] In subsequent data analyses it was assumed that the value of χ_f was independent of temperature and that only τ_f altered. T_1 values for free chloride (1 M) are given in Table I for each of the temperatures used in the present work together with the corresponding τ_f values.

4.2. Nonexponential Transverse Relaxation of Cl$^-$ Ions in Exchange with HSA. ^{35}Cl transverse relaxation measurements were conducted on null point samples both with and without SDS at 310 and 288 K at 29.4 MHz. The natural logarithm of the normalized magnetization is plotted against the echo time in the Hahn spin–echo rf pulse sequence in Figure 2. The nonexponential transverse relaxation is clearly evident from the nonlinearity of the plots, especially for exchange in the absence of SDS.

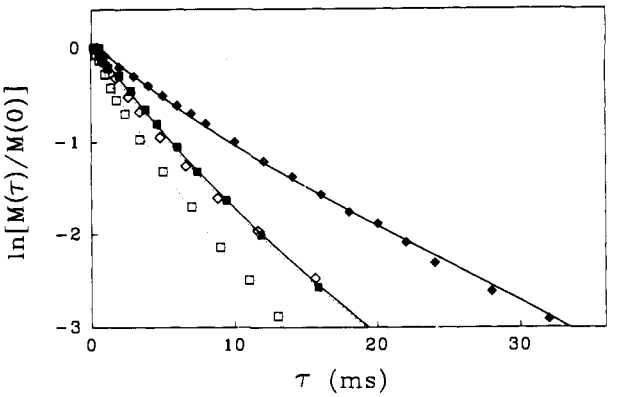

Figure 2. Plot of the logarithm of the normalized ^{35}Cl magnetization $M(\tau)/M(0)$ versus delay time (i.e., total echo time) τ in Hahn spin–echo rf pulse sequence conducted at 29.4 MHz for the null point samples both with (■) and without SDS (□) at 288 K and with (◆) and without SDS (◇) at 310 K. The curves represent regression of third-order polynomials through each of the four data sets. The nonlinearity of the plots is indicative of nonexponential relaxation.

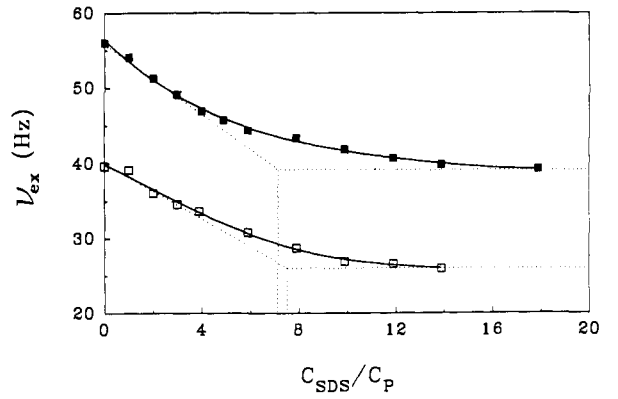

Figure 3. Effect of SDS addition on the excess ^{35}Cl line width ν_{ex} at 288 (■) and 298 K (□) in a sample containing 0.45 mM HSA, 50 mM Tris buffer, and 1 M Cl$^-$. The pH of the solution was 7.5 (uncorrected for isotope effect). The line width measurements were conducted at 29.4 MHz. The abscissa is given in terms of the molar ratio of SDS to HSA. The solid curves represent quartic polynomial regressions onto the data sets. Both SDS titrations gave the number of SDS-sensitive (i.e., strong) sites per HSA molecule to be 7 ± 1 (see dotted lines).

4.3. Weak Site. 4.3.1. SDS Titrations. The change in excess ^{35}Cl line width at 29.4 MHz in HSA solutions upon addition of SDS at 288 and 298 K is given in Figure 3. The SDS titrations at both temperatures give the number of strong binding sites to be 7 ± 1. Hence for a sample containing 1 M Cl$^-$ and 0.45 mM HSA in the limit of K_s approaching 0 (i.e., complete occupation of strong binding sites), an upper bound for p_s of 0.003 15 can be calculated using eq 3b. From the titration it can be seen that to completely inhibit chloride binding to the SDS-sensitive sites, the SDS:HSA ratio must be at least 7:1. Following the work of Norne and co-workers[8] and Scatchard and co-workers,[50] a thiocyanate titration was also undertaken at 8.8 MHz (data not shown). However, in contrast to the SDS titration and the results of Norne and co-workers,[8] addition of thiocyanate ion caused a much smaller reduction of the excess chloride line width.

4.3.2. Determination of τ_w and $p_w\chi_w^2$ from Null Point Spectra. ^{35}Cl longitudinal relaxation time measurements and null point spectra were conducted on the SDS-containing null point sample over a range of temperatures at 29.4 MHz. The longitudinal relaxation times are given in Table I, and the null point spectra together with their corresponding simulations are shown in Figure

(44) Jenkins, B. G.; Lauffer, R. B. *Mol. Pharmacol.* **1990**, *37*, 111–118.
(45) Van Geet, A. L. *Anal. Chem.* **1968**, *40*, 2227–2229.
(46) Van Geet, A. L. *Anal. Chem.* **1970**, *42*, 679–680.
(47) Hertz, H. G. *Prog. Nucl. Magn. Reson. Spectrosc.* **1967**, *3*, 159–230.
(48) Hertz, H. G. *Ber. Bunsenges. Phys. Chem.* **1973**, *77*, 531–540.
(49) Hertz, H. G. *Ber. Bunsenges. Phys. Chem.* **1973**, *77*, 688–697.
(50) Scatchard, G.; Scheinberg, I. H.; Armstrong, S. H., Jr. *J. Am. Chem. Soc.* **1950**, *72*, 540–546.

Figure 4. Experimental (top) and simulated (bottom) ^{35}Cl null point spectra of a null point sample containing SDS as a function of the τ delay time (ms) in the inversion–recovery rf pulse sequence at the temperatures shown. The spectra were acquired at 29.4 MHz. The line broadenings (Hz) added to the experimental spectra and to the simulated spectra are, respectively, at each temperature: 316 K, 3.0, 7.7; 310 K, 1.0, 4.6; 298 K, 4.0, 9.3; 288 K, 5.0, 12.1; 283 K, 4.0, 11.4; 278 K, 7.0, 12.2. The line broadenings were added to the experimental spectra to increase the apparent signal-to-noise ratio. The simulated spectra have line broadening added to account for (1) that added to the experimental spectra and (2) unspecified transverse relaxation (= the difference between the two line broadening factors), mainly magnetic inhomogeneity. The magnetic inhomogeneity was estimated by comparing Hahn spin–echo and line width measurements of protein-free saline solution. The magnetic inhomogeneity was found to account for less than 3 Hz of the observed line width at half height in the spectra. Relative to the fully relaxed spectrum (i.e., $\tau \geq 100$ ms) the ordinate magnification for the other spectra is 32.

4. The values of τ_w, $p_w\chi_w^2$, and an upper bound for p_w, given in Table I, were determined by simulating the null point spectra as described in Section 2.3. The upper bound for p_w was set to be the value which gave the ratio (intensity of the simulated null point spectra)/(intensity of the fully relaxed spectrum) to be 10% larger than the experimentally determined ratio. When p_w was set to this value the duration of the fine structure in the null point became slightly longer than that observed experimentally. The asymmetry parameter of the electric field gradient is implicitly contained in χ_w. Since it was only possible to determine an upper bound for p_w, χ_w could only be determined as the product $p_w\chi_w^2$.

4.3.3. Determination of the Enthalpy of Dissociation. ^{35}Cl longitudinal relaxation rate measurements at 29.4 MHz were conducted at various temperatures on a number of samples containing 1 M Cl^- and various HSA concentrations in the presence of sufficient SDS to inhibit the strong sites. As the upper bound of p_w (see Table I) is very small compared to the large free chloride concentration, p_f was set to 1. The free chloride relaxation rate

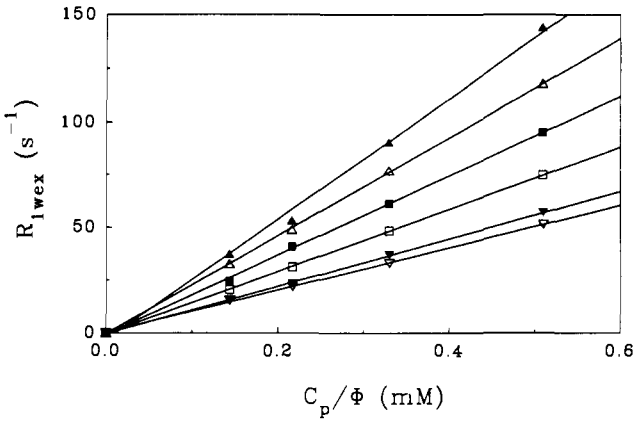

Figure 5. ^{35}Cl longitudinal excess relaxation rate R_{1wex} at 29.4 MHz versus C_P/Φ in the presence of sufficient SDS to block the strong binding sites at 278 (▲), 283 (△), 288 (■), 298 (□), 310 (▼), and 316 K (▽). Straight lines were regressed onto the data at each temperature. The slope of the lines at each temperature is $R_{1w}n_w\gamma_{Cl}/K_w$.

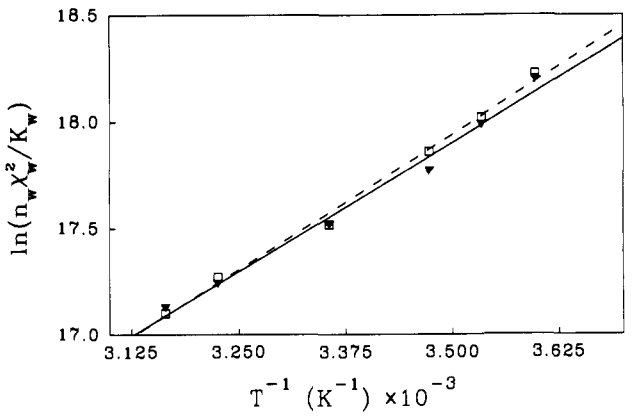

Figure 6. Plot of ln $(n_w\chi_w^2/K_w)$ versus T^{-1}. Values for $n_w\chi_w^2/K_w$ were determined from the temperature dependence of the excess longitudinal relaxation rates of samples containing SDS and different HSA concentrations (▼; see Figure 5) and from simulation of the null point spectra (□; see Figure 3 and Table I). The results of linear regression onto the data derived from the null point studies is denoted by the dashed line, and that onto the data derived from the protein concentration studies is denoted by the solid line.

was subtracted from that measured for the HSA containing samples, leaving the excess longitudinal relaxation rate for the weak site, R_{1wex}. $R_{1wex} = p_wR_{1w} \approx n_wa_{Cl}R_{1w}C_P/((K_w\Phi) + a_{Cl})C_{Cl})$, where R_{1w} is the relaxation rate at the weak binding site.[20] Since it was found that the relaxation rate was independent of chloride concentration for chloride concentrations between 0.1 and 1 M, it was inferred that $K_w \gg 1$. Since p_w is small, we have $a_{Cl} \approx \gamma_{Cl}C_{Cl}$, where γ_{Cl} is the mean chloride activity coefficient. Also it can be shown that $\Phi \approx 1$ (see Section 2.1 and Appendix 1), and so p_wR_{1w} can be further simplified to $R_{1w}n_w\gamma_{Cl}C_P/(K_w\Phi)$. Figure 5 is a plot of R_{1wex} versus C_P/Φ, and the slope of the plot is $R_{1w}n_w\gamma_{Cl}/K_w$. However, since we have already determined τ_w at each temperature (see Table I) and values of γ_{Cl} have been tabulated,[51,52] if we assume that $n_w\chi_w^2$ is temperature independent, we can simplify the slope even further to $n_w\chi_w^2/K_w$, where now only K_w is temperature dependent. Figure 6 is a plot of ln $(n_w\chi_w^2/K_w)$ versus inverse temperature. From linear regression of the data in Figure 6 and the relationship between the equilibrium constant and the standard molar Gibbs free energy, the enthalpy of dissociation of the weak site is determined to be 20.2 ± 2.0 kJ mol^{-1}. Since neither the number of SDS-insensitive chloride binding sites nor χ_w was known, the dissociation entropy could not be determined. As a cross check the term $n_w\chi_w^2/K_w$ was also determined directly from the values of $p_w\chi_w^2$ obtained from the null point simulations at each temperature. The results, which are also included in Figure 6, give the same value of the enthalpy of dissociation within experimental error.

(51) Stokes, R. H.; Robinson, R. A. *J. Am. Chem. Soc.* **1948**, *70*, 1870–1878.

(52) Harned, H. S.; Owen, B. B. *The Physical Chemistry of Electrolytic Solutions*, 3rd ed.; Reinhold Publishing Co.: New York, 1958; pp 489–506.

Table II. Longitudinal Relaxation Times (T_1) and Parameters Used from Simulating the ^{35}Cl Null Point Spectra of the Null Point Sample without SDS at Each Temperature[a]

T (K)	T_1 (ms)	$p_s\chi_s^2(1 + \eta^2/3 - A^2)\tau_{sf} \equiv C_1$[b] (rad s^{-1})	$p_s\chi_s^2A^2\tau_{ss} \equiv C_2$[b] (rad s^{-1})	τ_{ss}[c] (ns)	τ_{sf}[d] (ns)
316	11.9	264	3610	34	0.45
310	10.5	278	4710	35	0.50
298	8.1	383	6510	41	0.75
288	6.5	407	9890	51	0.90

[a] The parameters used to fit the weak site binding are given in Table I. [b] The values for C_1 and C_2 have about 5 and 2% error associated with them, respectively. [c] The τ_{ss} values have about 10% error associated with them. [d] Upper bound value.

4.4. Strong Sites. 4.4.1. Null Point Spectra. ^{35}Cl longitudinal relaxation time measurements and null point spectra were conducted on the null point samples without SDS over a range of temperatures. The null point spectra together with their corresponding simulations are given in Figure 7. The null point spectra were simulated as described in Section 2.3 together with the parameters previously determined for the weak site (see Table I) to give values for $p_s\chi_s^2(1 + \eta^2/3 - A^2)\tau_{sf}$, $p_s\chi_s^2A^2\tau_{ss}$, τ_{ss}, and an upper bound for τ_{sf} at each temperature. The results are given in Table II. The values for τ_w and $p_w\chi_w^2$ determined above were able to be used in simulating the null point spectra obtained in the absence of SDS since, with the exception of the SDS content, the sample composition was the same and the free chloride concentration was much greater than that bound to either of the two sites, so that the weak site characteristics were unchanged.

4.4.2. Determination of the Dissociation Constants of the Strong Sites. ^{35}Cl longitudinal relaxation rate measurements were performed at 29.4 MHz for a number of samples containing 0.45 mM HSA and various chloride concentrations at 310 K. Longitudinal relaxation measurements were also performed on a series of protein-free samples spanning the same chloride concentration, and interpolation was used to estimate the free relaxation rate at any point in the concentration range. This was done since the free chloride relaxation rate has a slight concentration dependence. Then longitudinal relaxation rates R_1 were simulated as described in Section 2.4. The results are plotted in Figure 8. The relaxation rate versus chloride concentration curve was then able to be simulated by setting K_s = 0.1 M and K_w = 50 M. However, due to the magnitude of K_w, providing that $K_w > 10$, a reasonable fit to the data was obtained. Thus, the population of the weak site was independent of the chloride concentrations used in the present study (see eq 3a).

4.5. Ionic Strength Effects on Chloride Binding. ^{35}Cl longitudinal relaxation measurements at 29.4 MHz were performed at 298 K on two sets of SDS-free samples containing 0.45 mM HSA and chloride concentrations ranging from 0.3 to 1 M. In one set of samples the ionic strength varied according to the chloride concentration. In the other set the ionic strength was adjusted with sodium sulfate so that each sample was equivalent in ionic strength to the 1 M chloride–HSA sample (i.e., without sodium sulfate). Sodium sulfate was chosen to adjust the ionic strength, as the sulfate ion has been shown to bind very weakly to HSA.[8] The measured longitudinal relaxation rates were dependent on the chloride concentration but independent of the sulfate concentration (data not shown). From this result it can be inferred that changes in ionic strength over the range of chloride concentrations used in the present work had negligible effect on chloride binding.

4.6. Isotopic and Frequency Dependence Cross Checks of the Relaxation Parameters. Since the values determined for τ_w, τ_{ss}, and the upper bound for τ_{sf} differ by orders of magnitude, the frequency dependence of the longitudinal and transverse relaxation of the strong and weak sites should be quite different. Two types

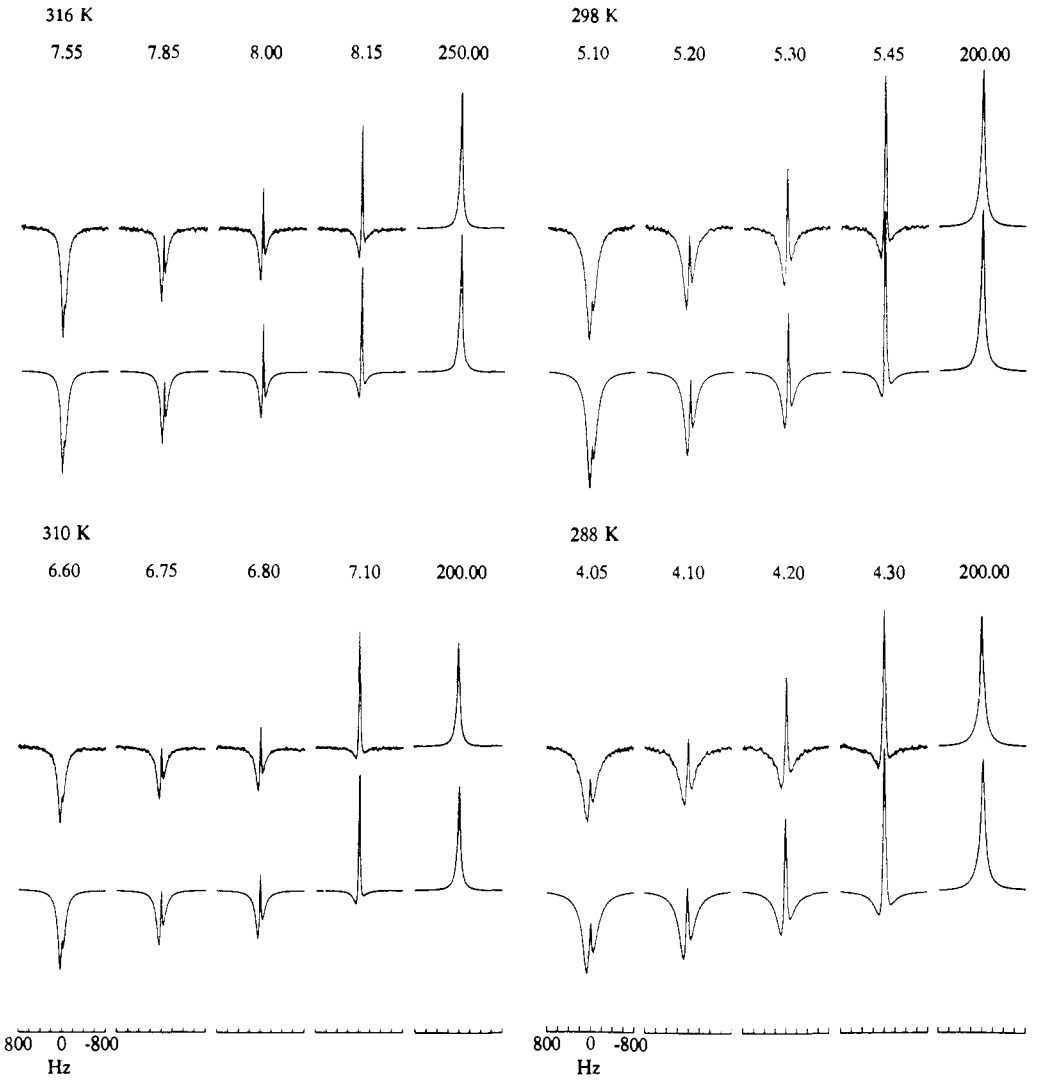

Figure 7. Experimental (top) and simulated (bottom) ^{35}Cl null point spectra at 29.4 MHz of a HSA sample at as a function of the τ delay time (ms) in the inversion–recovery rf pulse sequence at the temperatures shown. The line broadening (Hz) added to the experimental spectra and to the simulated spectra are, respectively, at each temperature: 316 K, 4.0, 5.4; 310 K, 4.0, 5.6; 298 K, 6.0, 7.5; 288 K, 6.0, 8.5. The reasons for using the line broadening have been mentioned in the caption to Figure 4. The magnetic inhomogeneity was found to account for less than 2.5 Hz of the measured line width at half height. Relative to the fully relaxed spectrum (i.e., $\tau \geq 200$ ms) the ordinate magnification for the other spectra is 32. Since the sample did not contain SDS the null point spectra observed contain contributions from both the strong and weak classes of binding sites. The parameters for simulating the spectra are given in Tables I and II.

Table III. Isotopic and Frequency Dependence Cross Checks at Various Temperatures of the Binding Parameters Determined for the Null Point Samples with and without SDS[a]

Freq (MHz)	T (K)	$T_{1\,expt\,-\,SDS}$[c] (ms)	$T_{1\,sim\,-\,SDS}$[c] (ms)	$T_{1\,expt\,+\,SDS}$[c] (ms)	$T_{1\,sim\,+\,SDS}$[c] (ms)
8.8	310	5.3	5.9	9.9	9.8
8.8	298	4.5	4.7	7.8	7.5
8.8	288	na[d]	na	5.5	5.4
24.5[b]	310	11.8	11.5	17.3	17.1
39.2	310	12.2	11.7	na	na

[a] Parameters are as given in Tables I and II. [b] The values at 24.5 MHz correspond to ^{37}Cl measurements. [c] The experimental longitudinal relaxation values ($T_{1\,expt}$) were simulated ($T_{1\,sim}$) as described in the text. [d] na = not applicable.

of cross check were performed: first ^{37}Cl null point and longitudinal relaxation measurements were conducted at 24.5 MHz, and second ^{35}Cl longitudinal relaxation measurements were conducted at 8.8 and 39.2 MHz.

4.6.1. ^{37}Cl Measurements at 24.5 MHz. ^{37}Cl null point spectra were acquired and longitudinal relaxation rates were measured at 298 K for the null point samples, both with and without SDS. After the differences in resonance frequency and quadrupole moment are accounted for, the parameters determined for the two classes of binding sites (see Tables I and II) correctly predict the ^{37}Cl longitudinal relaxation rate (see Table III), and good simulated fits to the null point spectra were obtained by varying the parameters by less than 10%. In comparison to ^{35}Cl, the smaller quadrupole moment of ^{37}Cl gives rise to the slower longitudinal relaxation for the null point samples, both with and without SDS.

4.6.2. ^{35}Cl Measurements at 8.8 MHz. Longitudinal relaxation measurements were conducted on the null point samples both with and without SDS at various temperatures; the experimentally determined and predicted values are given in Table III. The frequency dependence of the longitudinal relaxation of chloride ion binding is clearly evident by comparing the longitudinal relaxation rates of the samples, with and without SDS, with the relaxation rates given in Table I and II.

4.6.3. ^{35}Cl Measurements at 39.2 MHz. Longitudinal relaxation rate measurements were performed for a number of samples containing various chloride concentrations and 0.45 mM HSA

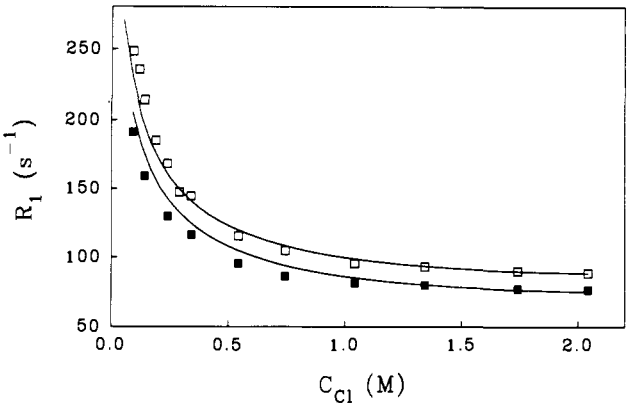

Figure 8. Plots of the longitudinal relaxation rate R_1 of ^{35}Cl at 29.4 (□) and 39.2 MHz (■) versus C_{Cl} for samples containing 0.45 mM HSA in the absence of SDS at 310 K. The simulations, represented by the solid curves, were performed as described in Section 2.4. The simulations provided a K_s value of 0.1 M and a K_w value of 50 M. The initial parts of the data sets, up to a chloride concentration of about 0.4 M, are dominated by the chloride ion interacting with the strong site; in the remainder of the data sets the contribution from the weak sites becomes more important. The assumption that the exchange of the chloride ions between the free and weak sites and between free and strong sites occurs independently is still valid at the lowest chloride concentrations since even at 0.092 mM Cl^- (the lowest concentration used in the present study), $p_s = 0.01$ and $p_w < 0.02$, hence $p_f \gg p_s, p_w$.

at 310 K. Longitudinal relaxation measurements were also performed on a series of HSA free samples spanning the same chloride concentration range and interpolation was used to estimate the free relaxation rate at any point in the concentration range. The values of the relaxation rate are plotted in Figure 8. The relaxation was then able to be successfully simulated (see Figure 8) using the parameters given in Tables I and II and the values for K_s and K_w determined above. The frequency dependence of the longitudinal relaxation is evident, especially in the early part of the curves where exchanges with the strong binding sites dominate the observed relaxation.

5. Discussion

Compared to previous studies of chloride binding to HSA, no approximations of the relaxation process such as in Bull's approach[24] were used. Also, in contrast to Bull's approach, our formulation remains valid if $\omega_0\tau_b > 1.5$. Additionally, compared to the method of Rose and Bryant[18] in which they use the ratio of the excess transverse relaxation rate to excess longitudinal relaxation rate, a well-defined T_2 is not a prerequisite in our formulation. For our experimental system, the transverse relaxation resulting from chloride ions in exchange with HSA was not well described by a single exponential (see Figure 2), and consequently the concept of a T_2 value was not well defined. Hence, apart from the line width measurements involved in the SDS titrations and the use of the spin–echo measurements of the free solution to determine the magnetic inhomogeneity, transverse relaxation measurements were not used.

Since the HSA-containing samples were all buffered to the same pH and the ionic strength was always greater than 0.1, the HSA molecules should be in the N conformation and the effective hydrodynamic shape of each albumin molecule should be constant.[7,53,54] Previous studies[55,56] have shown that the binding of SDS and Cl^- ions to HSA can cause a slight decrease in protein volume. However, this effect was not reflected in the NMR data we obtained. For example, in the SDS titrations (see Figure 3) the chloride excess line width showed only a monotonic decrease with increasing SDS concentration before leveling out. Also, in the experiment in which the chloride relaxation was measured with various chloride concentrations but with a constant HSA concentration (see Figure 8), the longitudinal relaxation showed a monotonic decrease with increasing chloride concentration. The results of the present work should be applicable to HSA in plasma since the pH in the present study is close to physiological pH and plasma has an ionic strength greater than 0.1. Since dimerization is known to occur at pH values less than 4,[19] most of the HSA should be monomeric. Tris was used as a buffer since it has been shown in previous studies[8,18] not to affect the binding of chloride ions to HSA. In previous NMR studies of chloride binding, activity effects were largely ignored. Here we have attempted to give a more complete accounting of activity effects. In the present work ionic strength effects were shown to be negligible over the range of ionic strengths used.

The good fit to the relaxation data obtained with our model and the appearance of the spectra show that the rate of chloride exchange is in fast exchange limit for all of the temperatures used in the present work. Intermolecular dipole–dipole relaxation, although very small compared to quadrupolar relaxation, was minimized by preparing all of the samples with D_2O instead of H_2O. The value of 1.7 MHz determined for χ_f is consistent with the value derived from Monte Carlo simulations[57] and 2.0 MHz derived from an electrostatic model.[48,49] In analyzing the relaxation data, it was assumed that the protein solutions were microheterogeneous,[8] such that the chloride ions behaved as in protein-free solution unless they were bound. The SDS titrations performed at 288 and 298 K both gave the number of strong binding sites to be 7 ± 1, in good agreement with previous NMR studies.[8,19] In addition, the agreement between results at the two temperatures showed that the number of SDS-sensitive binding sites was, within experimental error, independent of temperature. It was not possible, however, to enumerate the number of weak sites.

A single correlation time was sufficient for representing the fluctuation of the electric field gradient at the weak sites. Further, the small dissociation enthalpy precluded the use of the two-step model-free approach. However, for the strong sites the two-step model-free approach was used since it was not possible to simulate the "shoulders" (or "wings") of the null point spectra using a single correlation time. The effects of order on the chloride relaxation at the strong sites are apparent when comparing the shoulders of the null point spectra from three-site exchange with those from two-site exchange and noting the difference in abscissal scale. The two-step model allows for internal motion at the strong binding site without overinterpreting the relaxation data since the exact geometry of the binding sites is not known. A number of sets of parameters for the strong sites could be found that were consistent with the longitudinal and transverse relaxation times. However, only a much smaller group of these were able to fit the null point spectra. The dynamic frequency shift is almost totally dependent upon the value of τ_{ss} and hence provides a means for determining τ_{ss}. Also, an upper bound for τ_{sf} could be determined, beyond which the null point spectra could not be fitted (i.e., amplitude and the fine structure). From the values obtained for τ_{ss} and the upper bound obtained for τ_{sf} we can then show that, for example at 310 K and a spectrometer frequency of 29.4 MHz, $\omega_0\tau_{sf} \leq 0.1$ and $\omega_0\tau_{ss} \approx 6$, which are the conditions for the validity of eq 9. A useful comparison of the effects of correlation time on the fine structure of the null point can be made with Figure 3 from the work of Price and co-workers.[33] The frequency dependence of the chloride longitudinal relaxation shown in Figure 8, which is particularly evident in the initial part of the curves (up to a chloride concentration of 0.4 M) where the effects of the strong site dominate the relaxation ($K_s \approx 0.1$ M), is in agreement with the dispersion behavior for the τ_{ss} term, whereas in the later part of the curves, where the weak site contribution becomes more important, there is less frequency dependence, as expected since $\omega_0\tau_w \approx 0.6$ (310 K, 29.4 MHz).

(53) Raj, T.; Flygare, W. H. *Biochemistry* **1974**, *13*, 3336–3340.
(54) Squire, P. G.; Moser, P.; O'Konski, C. T. *Biochemistry* **1968**, *7*, 4261–4272.
(55) Benson, E. S.; Hallaway, B. E. *J. Biol. Chem.* **1970**, *245*, 4144–4149.
(56) Katz, S.; Shaw, M. E.; Chillag, S.; Miller, J. E. *J. Biol. Chem.* **1972**, *247*, 5228–5223.
(57) Engström, S.; Jönsson, B.; Jönsson, B. *J. Magn. Reson.* **1982**, *50*, 1–20.

Table IV. Comparison of Correlation Times for the Free Site (τ_f) and Weak Site (τ_w), and the Slow Correlation Time of the Strong Site (τ_{ss}) with Solution Viscosity (η_s) and Temperature

T (K)	η_s/T (mPa K^{-1})	τ_f (ps)	τ_w (ns)	τ_{ss} (ns)
316	2.64×10^{-3}	2.1	3.36	34
288	5.91×10^{-3}	4.1	3.55	51

Since the binding sites are spread (or at least not at well-defined sites) over the protein surface, an apparent reorientational correlation time for the overall motion of HSA (i.e., τ_{ss}) was assumed even though HSA is not spherical. The slow correlation time of the strong site is mainly dependent on the tumbling of the HSA molecule. The tumbling of HSA can be estimated using Debye theory[58]

$$\tau_{ss\text{-}rot} \equiv \frac{4\pi r_P^3 \eta_s}{3kT} \tag{10}$$

where k is the Boltzmann constant, T is temperature, and η_s is the solution viscosity. At 310 K the viscosity of a D_2O solution containing 1 M NaCl, 50 mM Tris, and 0.45 mM BSA was determined using an Ostwald viscometer with deionized water as reference[59] to be 0.931 mPa (unpublished result). Thus we calculate $\tau_{ss\text{-}rot}$ to be 40 ns which is in excellent agreement with our value of 35 ns (see Table II). If we assume that the temperature dependence of the viscosity of this solution is that of pure D_2O,[60] then at 298 K the viscosity should be approximately 1.19 mPa and so $\tau_{ss\text{-}rot}$ should be about 53 ns, which is in good agreement with our value of 41 ns. By way of comparison, the value for HSA calculated from dielectric measurements at 298 K[61] and converted to an NMR reorientational correlation time[62] is about 48 ns.

Previous NMR studies of chloride binding[8,19] have suggested that the strong binding sites consist of lysine and arginine residues with the correlation time for internal motion resulting from rotations around the carbon–carbon bonds in the lysyl or arginyl side chains.[19,22] Halle and Lindman[19] pointed out that this model for the strong binding sites agrees with the appreciable positive entropy change found upon chloride binding,[15] perhaps due to formation of chelated ion triplets[63] and the liberation of hydration water. If we accept this as the proper model of the strong binding site, then the order parameter can be related to the degree of freedom of motion of the amino acid side chain and τ_{sf} should reflect side-chain motion only. Typical effective correlation times for the internal motion of amino acid side chains range up to about 0.1 ns.[64,65] The small values of τ_{sf} obtained in the present work (it should be noted that our values of τ_{sf} are upper bounds) are then consistent with the motion of the chloride ion being bound to a rapidly moving side chain. In the present work, the values determined for τ_{sf} are at least 2 orders of magnitude smaller than the τ_{ss} values at all of the temperatures studied. By comparing our results with previous studies where only a single correlation time was used to describe binding at the strong site,[8,18] it can be seen that the apparent correlation times that they determined were in between τ_{ss} and τ_{sf}.

An interesting comparison between τ_f, τ_w, and τ_{ss} can be made by considering the effects of temperature and viscosity (see Table IV). The ratio of solution viscosity to temperature in going from 316 K down to 288 K increases by 124%. Over the same temperature range, τ_f and τ_{ss} increase by 95% and 50%, respectively; however, the increase for τ_w was much less. Thus by way of eq 10 there would appear to be a correlation beween τ_f and τ_{ss} with viscosity of the bulk solution and temperature, which is as expected for the free ion and for the overall reorientational motion of the HSA molecule. But the forces controlling τ_w must have a rather different activation energy than that involved with the viscosity of the bulk solution.

From thermodynamic arguments it has been suggested that the diffuse layer of the BSA molecule is the dominant locus for binding and not the surface.[66] If the diffuse layer is the weak binding site for chloride ions on HSA, then the value of the dissociation enthalpy of the weak sites determined (20.2 kJ mol^{-1}) is too small to account for binding of the chloride ion either to the protein surface or directly to the hydration layer of the protein. Also, the τ_w values we have determined are too fast to be consistent with the chloride ion being directly bound to the protein's hydration layer, where the water molecules are known to have correlation times up to an order of microseconds.[67] If the weak sites were constituted by the chloride ions being transient in the hydration layer (but not bound), it may explain why a previous study[8] revealed that anion binding to the weak class of binding sites nearly follows the lyotropic series.[36] It would also explain the small temperature dependence of τ_w, as it has been noted that the hydration layer of proteins does not behave like regular bulk water and instead remains fluid down to ≈200 K.[68]

Since only an upper bound for τ_{sf} could be determined for the temperatures studied and the order parameter A could not be determined, we were unable to use eq 9 to arrive at an estimate of χ_s; however, it would be possible to obtain an estimate if $\omega_0\tau_{sf}$ was in the dispersion region. We have refrained from using previously calculated values[22] or attempted to calculate χ_s since a number of important parameters are not known, including the dielectric constant of the medium.[22] As pointed out by Rose and Byrant,[18] the absence of covalent bonds between the exchanging ion and the binding site complicates the interpretation of χ_s. We could not determine χ_w since p_w could not be determined.

In comparison with previous work, this study presents more detailed results regarding the strong and the weak chloride binding sites. The study clearly demonstrates that analysis of null point spectra provides a convenient and experimentally simple means to study the binding of quadrupolar ions and allows more accurate estimates of the relavant correlation times. The traditional methods of analyzing quadrupolar relaxation in exchanging systems becomes more complicated as the extreme narrowing condition is even further violated. In particular the present work obviates the need to perform (unreliable) multiexponential regressions on T_1 or T_2 data, frequency dependence studies, or (more complicated) multiple-quantum experiments.[69] Also, it provides a much simpler means of observing the dynamic frequency shift than performing triple-quantum experiments.[70]

Appendix 1. Kinetics of Binding and Activity Affects

If we consider the binding of the chloride ions to the strong or weak sites to be independent (i.e., the binding to one class of site is unaffected by the number of Cl^- ions bound to the other class of site), then the population of n_s equivalent strong binding sites is given by[37]

$$p_s = \frac{n_s C_P [Cl]}{C_{Cl}(K_s + [Cl])} \tag{A.1.1}$$

where n_s is the number of strong binding sites, C_P is the total protein concentration, [Cl] is the free chloride concentration, C_{Cl} is the total chloride concentration, and K_s is the dissociation constant of Cl^- for the strong binding sites. On exchanging the

(58) Bloembergen, N.; Purcell, E. M.; Pound, R. V. *Phys. Rev.* **1948**, *73*, 679–712.
(59) *Handbook of Chemistry and Physics*; Weast, R. C., Ed.; CRC Press: Cleveland, OH, 1984.
(60) Mills, R. *J. Phys. Chem.* **1973**, *77*, 685–688.
(61) Moser, P.; Squire, P. G.; O'Konski, C. T. *J. Phys. Chem.* **1966**, *70*, 744–756.
(62) Hwang, J. S.; Mason, R. P.; Hwang, L. P.; Freed, J. H. *J. Phys. Chem.* **1975**, *79*, 489–511.
(63) Cotton, F. A.; Wilkinson, G. *Advanced Inorganic Chemistry*, 3rd ed.; Wiley: New York, 1972.
(64) Kay, L. E.; Torchia, D. A. *J. Magn. Reson.* **1991**, *95*, 536–547.
(65) Price, W. S.; Martenson, R. E.; Mendz, G. L. *Biochemistry* **1988**, *27*, 8990–8999.
(66) Fraaije, J. G. E. M.; Lyklema, L. J. *Biophys. Chem.* **1991**, *39*, 31–44.
(67) Kimmich, R.; Gneiting, T.; Kotitschke, K.; Schnur, G. *Biophys. J.* **1990**, *58*, 1183–1197.
(68) Kuntz, I. D.; Kauzmann, W. *Adv. Protein Chem.* **1974**, *28*, 239–345.
(69) Payne, G. S.; Styles, P. *J. Magn. Reson.* **1991**, *95*, 253–266.
(70) Eliav, U.; Shinar, H.; Navon, G. *J. Magn. Reson.* **1991**, *94*, 439–444.

subscript s for w, eq A.1.1 holds for the weak sites. In the present study we need to consider the activity, not the concentrations, of the species, and to do so we have adapted the work of Shearwin and Winzor.[71]

We assume that charge is conserved on successive chloride ion attachment to the protein molecule[72] and that, due to the small radius of the chloride ion relative to that of HSA, the HSA radius undergoes negligible change upon chloride binding. The bound population is then given by redefining Shearwin and Winzor's[71] eq 7 in terms of the dissociation constant and dividing by the total chloride concentration

$$p_s = \frac{n_s C_P[Cl]}{C_{Cl}(K_s\Phi + [Cl])} \quad (A.1.2)$$

where Φ is defined by

$$\Phi^{-1} = \exp\left[\alpha_{Cl,P}C_P - \frac{Z_{Cl}(1 + \kappa r_P + \kappa r_{Cl})[Z_P C_P + Z_{Cl}C_{Cl}]}{2I(1 + \kappa r_P)(1 + \kappa r_{Cl})}\right] \quad (A.1.3)$$

$\alpha_{Cl,P}$ is the second virial coefficient of the system considering the interactions of Cl^- with HSA, Z_P is the net charge on HSA (= −23), Z_{Cl} is the charge of the chloride ion, r_P is the effective radius of HSA (3.53 nm), r_{Cl} is the radius of the chloride ion (0.18 nm), and κ is the inverse of the Debye length. Using the statistical mechanical basis of excluded volume, $\alpha_{Cl,P}$ is related to the molecular parameters by the equation[73]

$$\alpha_{Cl,P} = U_{Cl,P} - M_P\nu_P + \frac{Z_P Z_{Cl}(1 + \kappa r_P + \kappa r_{Cl})[Z_P C_P + Z_{Cl}C_{Cl}]}{2I(1 + \kappa r_P)(1 + \kappa r_{Cl})} \quad (A.1.4)$$

The covolume $U_{Cl,P}$ is given by $4\pi N(r_P + r_{Cl})^3/3$, where N is Avogardro's number and ν_P is the partial specific volume of HSA (1.67 mL g^{-1}). The second term on the right-hand side denotes the molar volume of the anhydrous albumin, and the final term accounts for charge–charge interactions. Since the formulation of Winzor and Shearwin[71] does not account for nonideality of the chloride ion, we replace [Cl] by the activity[51,52] of Cl in eq A.1.2.

Appendix 2. State Multipoles

A rank k-state multipole with tensorial component m is defined by

$$\sigma^k_m \equiv \sum_\alpha \sum_{\alpha'} \rho_{\alpha\alpha'}(-1)^{1-\alpha}\left(2k+1\right)^{1/2}\begin{pmatrix} I & I & k \\ \alpha & -\alpha' & -m \end{pmatrix} \quad (A.2.1)$$

where $\rho_{\alpha\alpha'}$ are density matrix element, I is the spin quantum number, and $\begin{pmatrix} I & I & k \\ \alpha & -\alpha' & -m \end{pmatrix}$ is a $3-j$ symbol.[74,75] State multipoles have two major advantages, the first being that the state multipoles can be associated with measurable spectral magnetizations. For example, σ^1_0 corresponds to the longitudinal magnetizations, and σ^1_1 (or σ^1_{-1}) corresponds to the transverse magnetizations. In general, σ^k_m corresponds to k-quantum coherence for $m = 1$ or -1, and for a multispin system it corresponds to k-spin order for $m = 0$. The second advantage is that state multipoles transform very simply under rotation since each multipole transforms as a component of the full rotation group. For example, an on-resonance radio frequency pulse transforms the state multipole components according to the relation[33,76]

$$(\sigma^+)^k_m = \sum_n D^k_{mn}(\phi - \pi/2, \theta, \pi/2 - \phi)(\sigma^-)^k_n \quad (A.2.2)$$

where $D^k_{mn}(\alpha,\beta,\gamma)$ is a Wigner rotation matrix element,[74,75] θ is the radio frequency pulse angle, ϕ is the radio frequency phase angle associated with the θ angle pulse with respect with respect to the x axis in the rotating frame, and the superscript +/− indicates the state multipoles after/before the pulse.

Appendix 3. Two-Step Model-Free Approach

Here we modify the approach of Halle and Wennerström[43] for use in the present study. Since in our study we were concerned only with an atomic system (i.e., chloride ions) instead of Halle and Wennerström's[43] molecular system (i.e., water molecules), we have omitted their molecular frame in describing the reorientational motion of the Cl^- ions at the strong binding sites. After some algebra it can be shown that the spectral density functions defined previously[43] are given for the present case by

$$J_n \equiv \int_0^\infty G(t)\cos(n\omega_0 t)dt = \frac{3}{10}(eq)^2\left[\left(1 + \frac{\eta^2}{3} - A^2\right)J_{nf} + A^2 J_{ns}\right] \quad (A.3.1)$$

and

$$Q_n \equiv \int_0^\infty G(t)\sin(n\omega_0 t)dt = \frac{3}{10}(eq)^2\left[\left(1 + \frac{\eta^2}{3} - A^2\right)Q_{nf} + A^2 Q_{ns}\right] \quad (A.3.2)$$

where

$$J_{nf} = \frac{\tau_{sf}}{1 + (n\omega_0\tau_{sf})^2},\ J_{ns} = \frac{\tau_{ss}}{1 + (n\omega_0\tau_{ss})^2},$$

$$Q_{nf} = \frac{n\omega_0\tau_{sf}^2}{1 + (n\omega_0\tau_{sf})^2},\ \text{and}\ Q_{ns} = \frac{n\omega_0\tau_{ss}^2}{1 + (n\omega_0\tau_{ss})^2}$$

If A is set to 0, then the definitions given for J_n and Q_n agree with those given in our previous work.[33]

Acknowledgment. Support of this work by grants from the National Science Council of the Replublic of China is gratefully acknowledged. Dr. G. B. Ralston and Dr. A. P. Minton are thanked for discussions on activity effects in protein solutions.

(71) Shearwin, K. E.; Winzor, D. J. *Biophys. Chem.* **1990**, *36*, 235–243.
(72) Ford, C. L.; Winzor, D. J. *Biochim. Biophys. Acta* **1982**, *703*, 109–112.
(73) Wills, P. R.; Nichol, L. W.; Siezen, R. J. *Biophys. Chem.* **1980**, *11*, 71–82.
(74) Rose, M. E. *Elementary Theory of Angular Momentum*; Wiley: New York, 1957.
(75) Brink, D. M.; Satchler, G. R. *Angular Momentum*; University Press: Oxford, 1962.
(76) Furō, I.; Halle, B.; Wong, T. C. *J. Chem. Phys.* **1988**, *89*, 5382–5397.